Proceedings of the 9th International Conference on Power Electronics (ECCE Asia 2015), Seoul, South Korea, June 1-5, 2015

Control of the Input Characteristic and the Displacement Factor of Uni- and Bidirectional SWISS Rectifier for Symmetrical and Unsymmetrical Three-Phase Mains

L. Schrittwieser,
M. F. Vancu,
J. W. Kolar,
T. B. Soeiro

9th International Conference on Power Electronics-ECCE Asia
June 1 - 5, 2015 / 63 Convention Center, Seoul, Korea

Control of the Input Characteristic and the Displacement Factor of Uni- and Bidirectional SWISS Rectifier for Symmetrical and Unsymmetrical Three-Phase Mains

L. Schrittwieser*, M. F. Vancu*, J. W. Kolar* and T. B. Soeiro†
*Power Electronic Systems Laboratory, ETH Zurich, Switzerland, Email: schrittwieser@lem.ee.ethz.ch
†ABB Switzerland Ltd., Corporate Research, 5405 Baden-Dättwil, Switzerland

Abstract—**This paper introduces a phase-oriented control strategy for the uni- and bidirectional three-phase, buck-type SWISS Rectifier. It allows phase shifted sinusoidal input currents which enable the generation of capacitive or inductive reactive power at the converter's AC grid interface. Furthermore, the operation of the SWISS Rectifier with unsymmetrical AC mains voltages is analyzed. Modifications of the control structure, allowing constant AC input power or ohmic mains behavior even with unsymmetrical AC voltages are presented. Simulations and measurements taken on a 7.5 kW bidirectional SWISS Rectifier hardware prototype demonstrate the validity of the theoretical considerations.**

I. Introduction

The charging of Electric Vehicle batteries requires a conversion of the three-phase AC mains' voltage into an adjustable DC output voltage level [1]. This is also the case for future LV DC distribution systems and DC micro girds which typically require a connection to the existing AC utility grid [2]. Similar DC distribution systems, with a voltage of $\approx 400\,\mathrm{V}$ DC, are expected to reduce the power consumption and capital cost of data centers and telco sites by reducing the number of energy conversion stages [3][4].

Typically, if the voltage on the DC bus is lower than the full-wave rectified AC voltage, two stage systems are used. These consist of a front-end boost type power factor correction (PFC) stage with a $700\,\mathrm{V} - 800\,\mathrm{V}$ DC output connected in series with a DC-DC converter to achieve the desired lower DC bus voltage. For these applications buck-type PFC converters, like the SWISS Rectifier, are an alternative, allowing a single-stage energy conversion between the three-phase mains and a DC bus with lower voltage.

The schematic of the unidirectional SWISS Rectifier, as introduced in [5] and [6], is shown in **Fig. 1**. It consists of an AC side low-pass input filter, an Input Voltage Selector (IVS), two DC-DC buck converters and a DC output capacitor C_{pn}. Additional capacitors C'_{f} are used to minimize the commutation inductance of the buck converters. The IVS uses a three-phase full-wave diode bridge and a third harmonic injection network to connect the input phase with highest potential to node x, the one with lowest potential to node z and the remaining phase to node y. Therefore the injection network's switches $\mathrm{S}_{\bar{\mathrm{a}}\mathrm{y}\bar{\mathrm{a}}}$, $\mathrm{S}_{\bar{\mathrm{b}}\mathrm{y}\bar{\mathrm{b}}}$ and $\mathrm{S}_{\bar{\mathrm{c}}\mathrm{y}\bar{\mathrm{c}}}$ are switching with twice the mains frequency.

A bidirectional extension of the SWISS Rectifier, introduced in [7], is shown in **Fig. 2**. The additional switches allow a power transfer from the DC to the AC side. In order to enable this feedback of power into the mains the current in the DC-DC converter inductors L_{p} and L_{n} needs to be reversed. Therefore, switches $\mathrm{S}_{\bar{\mathrm{p}}\mathrm{y}}$ and $\mathrm{S}_{\mathrm{y}\bar{\mathrm{n}}}$ are connected in parallel with the buck converter diodes $\mathrm{D}_{\mathrm{y}\bar{\mathrm{p}}}$ and $\mathrm{D}_{\bar{\mathrm{n}}\mathrm{y}}$ of the unidirectional SWISS Rectifier. Furthermore, the diode bridge of the IVS is extended with six additional switches ($\mathrm{S}_{\mathrm{x}\bar{k}}$, $\mathrm{S}_{\bar{k}\mathrm{z}}$, $\bar{k} \in \{\bar{a}, \bar{b}, \bar{c}\}$) in order to allow it to conduct the reversed currents $i_{\mathrm{x}} < 0$ and $i_{\mathrm{z}} > 0$. These additional switches are turned on when their antiparallel diode would conduct in the unidirectional SWISS Rectifier. Hence, the switches $\mathrm{S}_{\mathrm{x}\bar{\mathrm{a}}}$, $\mathrm{S}_{\mathrm{x}\bar{\mathrm{b}}}$, $\mathrm{S}_{\mathrm{x}\bar{\mathrm{c}}}$, $\mathrm{S}_{\bar{\mathrm{a}}\mathrm{z}}$, $\mathrm{S}_{\bar{\mathrm{b}}\mathrm{z}}$ and $\mathrm{S}_{\bar{\mathrm{c}}\mathrm{z}}$ are operated at mains frequency.

This paper presents a phase-oriented PWM control method

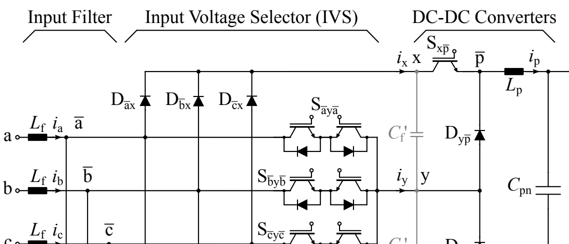

Fig. 1. Circuit topology of the unidirectional SWISS Rectifier, which is capable of AC-to-DC power transfer only. It consists of a low-pass input filter, a mains frequency commutated Input Voltage Selector (IVS) and two buck-type DC-DC converters as introduced in [5].

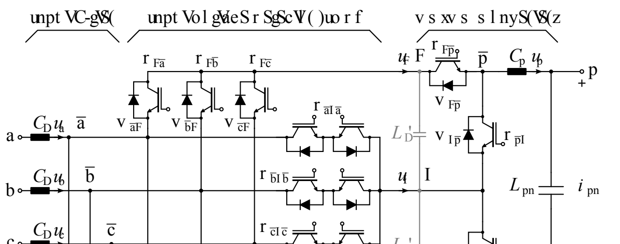

Fig. 2. Schematic of the bidirectional SWISS Rectifier, which is capable of AC-to-DC and DC-to-AC power transfer. It consists of a low-pass input filter, a bidirectional Input Voltage Selector (commutated at mains frequency) and two bidirectional DC-DC converters [7].

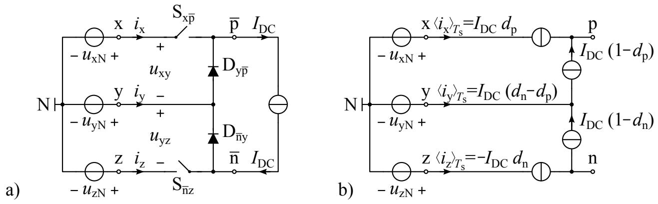

Fig. 3. Simplified schematics of the unidirectional SWISS Rectifier. In a) the mains, input filter and IVS are replaced with equivalent voltage sources and the output inductors (L_p and L_n) are replaced with a constant current source. By averaging over one switching frequency period T_s the schematic shown in b) results where d_p is the duty cycle of $\mathrm{S_{x\bar{p}}}$ and d_n is the duty cycle of $\mathrm{S_{\bar{n}z}}$.

for the uni- and bidirectional SWISS Rectifier, which allows the generation of reactive power on the AC side input. It is described in **Section II**, following an analysis of the topology's reactive power generation limits. Furthermore analytical formulas for the current stresses of the semiconductors and passive components are derived. Simulation results are included to demonstrate the theoretical considerations. In **Section III** the operation of the SWISS Rectifier with unsymmetrical mains voltages is analyzed. An extension to the basic control structure is proposed which achieves ohmic behavior at the AC input even with unsymmetrical mains voltages. **Section IV** presents measurements taken on a 7.5 kW SWISS Rectifier hardware prototype which demonstrate the feasibility of the proposed concepts.

II. Operation with Phase Shifted AC Currents

As shown in [6], the SWISS Rectifier's DC-DC converters can be controlled such that the rectifier system's AC side input currents $i_\mathrm{a,b,c}$ are sinusoidal and in phase with the grid voltages. This can also be seen from the simplified schematic shown in **Fig. 3**. By assuming a constant DC output inductor current I_DC the local average $\langle i_\mathrm{x}\rangle_{T_\mathrm{s}}$ of i_x over one switching frequency period T_s, can be calculated as

$$\langle i_\mathrm{x}\rangle_{T_\mathrm{s}} = I_\mathrm{DC}\, d_\mathrm{p}\ , \tag{1}$$

where d_p is the duty cycle of $\mathrm{S_{x\bar{p}}}$. This implies that d_p can be used to control the local average of the input current i_x and hence the current the mains' phase connected to node x via the IVS. In an analog way $\mathrm{S_{\bar{n}z}}$ and d_n can be used to control i_z. Therefore d_p and d_n can be used to achieve sinusoidal AC input currents and to create reactive power at the system's AC input by controlling the input displacement factor. However, the generation of reactive power reduces the output voltage range as will be shown in the following.

A. Output Voltage Range

In order to achieve sinusoidal AC side input currents the duty cycle signals d_p and d_n have to be piecewise sinusoidal as described above. Furthermore, the two DC-DC converters create a constant DC output voltage from the three output voltages of the IVS (u_xN, u_yN, u_zN),

$$\langle u_\mathrm{\bar{p}N}\rangle_{T_\mathrm{s}} = u_\mathrm{yN}\,(1-d_\mathrm{p})\ +\ u_\mathrm{xN}\,d_\mathrm{p}\ , \tag{2}$$

$$\langle u_\mathrm{\bar{n}N}\rangle_{T_\mathrm{s}} = u_\mathrm{yN}\,(1-d_\mathrm{n})\ +\ u_\mathrm{zN}\,d_\mathrm{n}\ , \tag{3}$$

where $\langle u_\mathrm{\bar{p}N}\rangle_{T_\mathrm{S}}$ is the local average of $u_\mathrm{\bar{p}N}$ over one switching perdio T_s. Note that $\langle u_\mathrm{\bar{p}N}\rangle_{T_\mathrm{S}}$ is bounded by u_xN and u_yN, while $\langle u_\mathrm{\bar{n}N}\rangle_{T_\mathrm{S}}$ is bounded by u_yN and u_zN. A drawing of the resulting signals is shown in **Fig. 4 a-c)**.

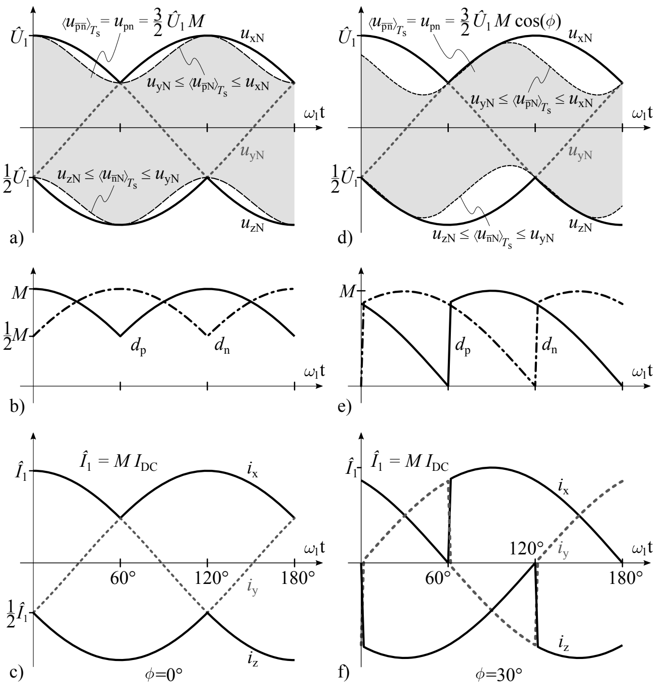

Fig. 4. Comparison of in-phase AC input currents (a-c) and phase shifted AC input currents (d-f). a) and d) show the IVS output voltages and DC output voltage range. b) and e) show the duty cycle signals d_p and d_n which generate the AC input currents shown in c) and f).

For ohmic mains behavior the DC output voltage u_pn is therefore limited to $1.5\,\hat{U}_1$, where $\hat{U}_1$ denotes the amplitude of the mains' phase voltage (cf. **Fig. 4 a**). Note that the amplitude of the two duty cycle signals (d_p, d_n) defines the system's modulation index $M \in [0;1]$ which sets the DC output voltage, $u_\mathrm{pn} = 1.5\,\hat{U}_1\,M$.

If the AC side input currents are phase shifted by the angle ϕ (w.r.t. the mains' phase voltages) this implies that the duty cycle signals have to be shifted as well (cf. **Fig. 4 e)**. Applying the phase shifted d_p and d_n to the input voltages u_xN, u_yN and u_zN results in a reduced output voltage of

$$u_\mathrm{pn} = \langle u_\mathrm{\bar{p}\bar{n}}\rangle_{T_\mathrm{s}} = \frac{3}{2}\,I_\mathrm{DC}\,M\,\cos(\phi) \qquad M\in[0;1]\ , \tag{4}$$

which can also be seen in **Fig. 4 d)**.

B. Reactive Power Generation Limits

In the **Fig. 4 d-f)** the AC side input phase currents are shifted by $\phi = 30°$. Note that either d_p or d_n reaches zero at every mains' voltage sector boundary (i.e. every 60°). Any further increase of ϕ would result in negative duty cycle values and hence in a low frequency distortion of the AC side input currents. In order to avoid these distortions of the AC input currents, ϕ has to be limited to

$$-\frac{\pi}{6} \le \phi \le \frac{\pi}{6}\ . \tag{5}$$

Assuming a constant DC output current I_DC and neglecting any losses in the semiconductors and filter components the active and reactive power at the converter's mains interface can be drived as

$$P = \frac{3}{2}\,\hat{U}_1\,I_\mathrm{DC}\,M\,\cos(\phi) = S_\mathrm{max}\,M\,\cos(\phi)\ , \tag{6}$$

$$Q = \frac{3}{2}\,\hat{U}_1\,I_\mathrm{DC}\,M\,\sin(\phi) = S_\mathrm{max}\,M\,\sin(\phi)\ . \tag{7}$$

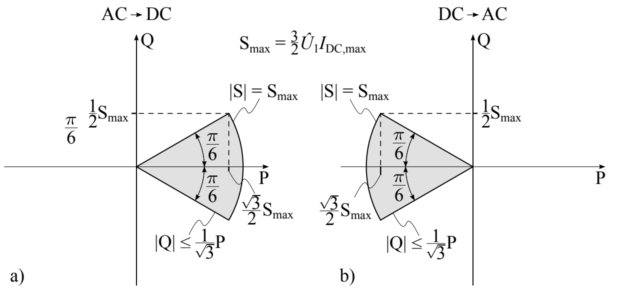

Fig. 5. Reactive power Q generation limits for the uni- and bidirectional SWISS Rectifier as a function of active power P and apparent power limit S_{max} for a) AC-to-DC power transfer and b) DC-to-AC power transfer.

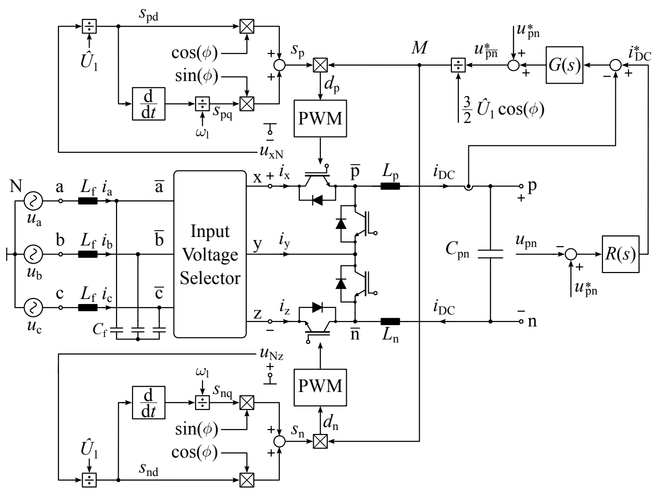

Fig. 6. Phase voltage oriented control structure for the bidirectional SWISS Rectifier. The sinusoidal AC side input currents are phase shifted by ϕ with $|\phi| \leq 30°$.

This leads to the reactive power generation limits shown in **Fig. 5**. Note that the same reactive power generation limits exist for the six-switch buck-type PWM converter [8].

C. Control Structure

The phase voltage oriented control structure shown in **Fig. 6** allows the generation of reactive power on the rectifier's AC side using the considerations given above. As in [5] An outer loop voltage controller $R\,(s)$ is used in order to control the DC output voltage u_{pn} by creating a reference signal i^*_{DC} for the underlying current controller $G\,(s)$. The output voltage reference u^*_{pn} is added as a feedforward signal to the current controller's output to calculate the DC-DC converter output voltage reference $u^*_{\bar{p}\bar{n}}$. Dividing by the maximum DC voltage $(1.5\,\hat{U}_1\cos(\phi)$, cf. (4)) yields the modulation index M.

In order to achieve sinusoidal AC input currents, M is multiplied with piecewise sinusoidal, unity amplitude shaping signals s_p and s_n. An illustration of these signals (for $\phi = 30°$) is shown in **Fig. 7**. The signals s_p and s_n are calculated as weighted sum from the corresponding shaping signals for ohmic behavior (s_{pd}, s_{nd}) and a signal leading by 90° (s_{pq}, s_{nq}) as shown in **Fig. 6**. This control structure ensures that the duty cycle signals d_p and d_n will not exceed the converter's linear operating range given conditions (4) and (5) are met.

Figure 8 shows simulation results for a 7.5 kW SWISS Rectifier with key parameters as listed in **Table I**. For the first 20 ms the rectifier operates with $\phi = -30°$ which results in inductive behavior. From $t = 20$ ms to $t = 40$ ms no phase shift is applied ($\phi = 0°$) which results in AC currents which are in phase with the phase voltages. For $t > 40$ ms the AC currents lead the voltage ($\phi = 30°$), which results in capacitive behavior.

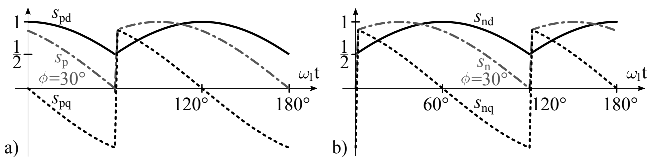

Fig. 7. Duty cycle shaping signals s_p and s_n used to achieve sinusoidal, phase shifted ($\phi = 30°$) inputs currents. The phase shift can be adjusted by calculating a weighted sum of active (s_{pd}, s_{nd}) and reactive (s_{pq}, s_{nq}) shaping signals as shown in **Fig. 6**.

Simulation results for the same system, but with DC-to-AC power transfer, are shown in **Fig. 9**. Again, the converter can be operated with a phase shift of up to $\phi = \pm 30°$ with sinusoidal input currents. This allows the generation of reactive power on the AC side, which e.g. could be used to compensate the reactive power demand of the AC grid filter. For example, a similar approach as presented in [9] for the six switch rectifier could be used.

TABLE I
SPECIFICATIONS OF SIMULATED SWISS RECTIFIER

AC Input Voltage (Line to Neutral)	$U_1 = 230$ V rms
AC Input Frequency	$\omega_1 = 50$ Hz
Switching Frequency	$f_s = 36$ kHz
Nominal DC Voltage	$U_{pn} = 400$ V
DC Link Capacitor	$C_{pn} = 470\,\mu$F
DC Link Inductor	$L_p = L_n = 250\,\mu$H
DC Output Power	$P = 7.5$ kW
AC Filter Inductor	$L_f = 120\,\mu$H
AC Filter Capacitor	$C_{\bar{a},\bar{b},\bar{c}} = 4.4\,\mu$F

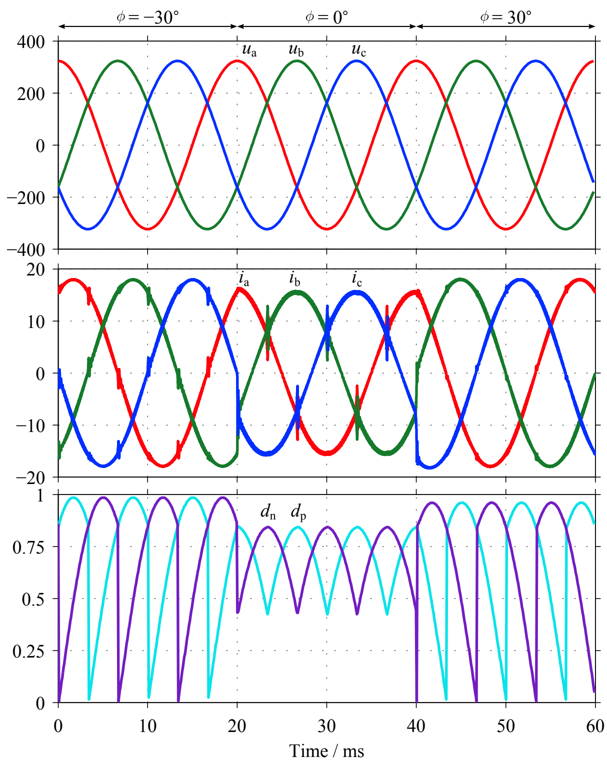

Fig. 8. Simulated mains voltages $u_{a,b,c}$, input currents $i_{a,b,c}$ and DC-DC converter duty cycles d_p and d_n for $\phi = -30°$ (inductive), $\phi = 0°$ (ohmic) and $\phi = 30°$ (capacitive) AC side currents for AC-to-DC power transfer.

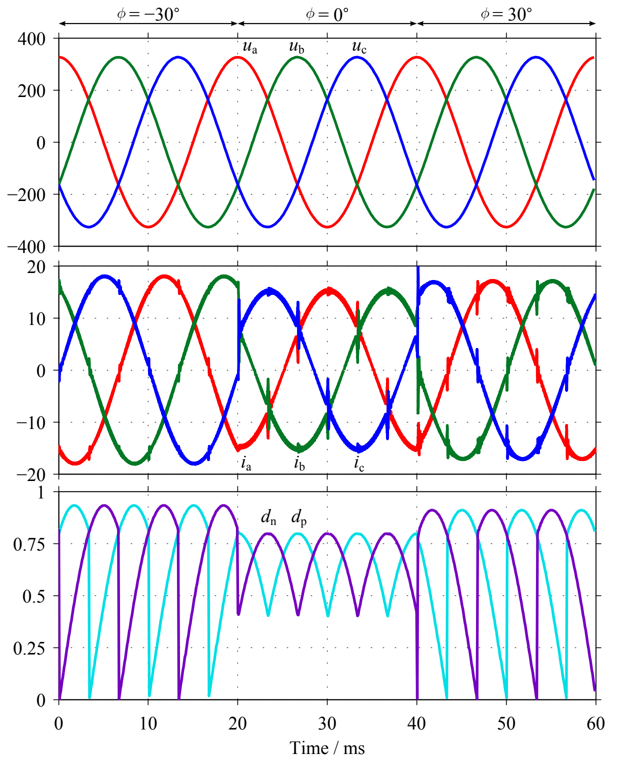

Fig. 9. Simulated grid voltages $u_{\mathrm{a,b,c}}$, input currents $i_{\mathrm{a,b,c}}$ and DC-DC converter duty cycles d_{p} and d_{n} for $\phi = -30°$ (capacitive), $\phi = 0°$ (ohmic) and $\phi = 30°$ (inductive) AC side currents for DC-to-AC power transfer.

D. Current Stresses

In order to select components for a SWISS Rectifier design the current stresses of the passive components and the semiconductor devices have to be calculated. This section extends the analytical equations presented in [6] for phase shifted AC input currents. The following analysis assumes AC-to-DC power transfer, however, analog equations can be derived for DC-to-AC power transfer as well. Furthermore, any switching frequency ripple in the DC side filter inductors $\mathrm{L_p}$ and $\mathrm{L_n}$ and in the AC side filter inductors $\mathrm{L_f}$ is neglected.

1) DC-DC Converters: In AC-to-DC power transfer only the switches $\mathrm{S_{x\bar{p}}}$ and $\mathrm{S_{\bar{n}z}}$ and the diodes $\mathrm{D_{y\bar{p}}}$ and $\mathrm{D_{\bar{n}y}}$ conduct current. The switch $\mathrm{S_{x\bar{p}}}$ conducts the DC output current I_{DC} when it is turned on while the diode $\mathrm{D_{y\bar{p}}}$ conducts while $\mathrm{S_{x\bar{p}}}$ is off. Neglecting the output current's switching frequency ripple this can be expressed as

$$i_{\mathrm{Sx\bar{p}}} = \begin{cases} I_{\mathrm{DC}} & \text{if } \mathrm{S_{x\bar{p}}} \text{ is on} \\ 0 & \text{if } \mathrm{S_{x\bar{p}}} \text{ is off} \end{cases} \tag{8}$$

$$i_{\mathrm{Dy\bar{p}}} = I_{\mathrm{DC}} - i_{\mathrm{Sx\bar{p}}}\,. \tag{9}$$

In order to calculate the rms and average current of the DC-DC converter semiconductors the duty cycle d_{p} of $\mathrm{S_{x\bar{p}}}$ is required. Using **Fig. 6** the positive side duty cycle can be derived as

$$d_{\mathrm{p}}(\omega t) = M\left[\cos(\phi)\cos(\omega t) - \sin(\phi)\sin(\omega t)\right] \tag{10}$$

$$\text{for } -\frac{\pi}{3} \leq \omega t \leq \frac{\pi}{3}\,. \tag{11}$$

Using (8) the rms current conducted by $\mathrm{S_{x\bar{p}}}$ can be calculated as

$$I_{\mathrm{Sx\bar{p},rms}} = I_{\mathrm{DC}}\sqrt{\frac{3\sqrt{3}}{2\pi}M_{\mathrm{d}}} \quad \forall\, \phi \in \left[-\frac{\pi}{6};\frac{\pi}{6}\right], \tag{12}$$

where M_{d} denotes the active power modulation index, defined as

$$M_{\mathrm{d}} = M\cos(\phi) = \frac{P}{S_{\mathrm{max}}}\,. \tag{13}$$

Similarly the average current in $\mathrm{S_{x\bar{p}}}$ can be found by integration as

$$I_{\mathrm{Sx\bar{p},avg}} = I_{\mathrm{DC}}\frac{3\sqrt{3}}{2\pi}M_{\mathrm{d}} \quad \forall\, \phi \in \left[-\frac{\pi}{6};\frac{\pi}{6}\right]. \tag{14}$$

As the diode $\mathrm{D}_{y\bar{p}}$ conducts the DC current I_{DC} whenever $\mathrm{S}_{x\bar{p}}$ is turned off its rms and average current can directly be derived using (12) and (14),

$$I_{\mathrm{Dy\bar{p},rms}} = I_{\mathrm{DC}}\sqrt{1 - \frac{3\sqrt{3}}{2\pi}M_{\mathrm{d}}} \quad \forall\, \phi \in \left[-\frac{\pi}{6};\frac{\pi}{6}\right], \tag{15}$$

$$I_{\mathrm{Dy\bar{p},avg}} = I_{\mathrm{DC}}\left(1 - \frac{3\sqrt{3}}{2\pi}M_{\mathrm{d}}\right) \quad \forall\, \phi \in \left[-\frac{\pi}{6};\frac{\pi}{6}\right]. \tag{16}$$

Due to the symmetry of the positive and the negative side DC-DC converters the same current stresses result for $\mathrm{S_{\bar{n}z}}$ and $\mathrm{D_{\bar{n}y}}$

Note that the rms and average currents in the DC-DC converter switches and diodes do not depend directly on ϕ but are a function of the active power P. This implies that the current stresses, and hence the conduction losses, in the DC-DC converter semiconductors are typically independent of the reactive power Q generated on the AC side. As the DC-DC converter switching losses depend on the input voltages u_{xy}, u_{yz} and the DC side output current I_{DC} they do not depend on Q either. Hence only active power is processed by the DC-DC converters.

2) IVS: As can be seen from the schematic shown in **Fig. 1** exactly one of the three positive side rectifier diodes ($\mathrm{D_{\bar{a}x}}$, $\mathrm{D_{\bar{b}x}}$, $\mathrm{D_{\bar{c}x}}$) is conducting during each gird voltage sector. Therefore, the forward biased diode conducts the same current as the switch $\mathrm{S_{x\bar{p}}}$. The rms and average current stress of the rectifier diodes can then be calculated using (12) and (14),

$$I_{\mathrm{D\bar{k}x,rms}} = I_{\mathrm{DC}}\sqrt{\frac{\sqrt{3}}{2\pi}M_{\mathrm{d}}} \quad \forall\, \bar{k} \in \{\bar{a},\bar{b},\bar{c}\}\,, \tag{17}$$

$$I_{\mathrm{D\bar{k}x,avg}} = I_{\mathrm{DC}}\frac{\sqrt{3}}{2\pi}M_{\mathrm{d}} \quad \forall\, \bar{k} \in \{\bar{a},\bar{b},\bar{c}\}\,. \tag{18}$$

Due to the circuit's symmetry the same equations result for the negative side diodes $\mathrm{D_{z\bar{a}}}$, $\mathrm{D_{z\bar{b}}}$, $\mathrm{D_{z\bar{c}}}$.

In the third harmonic injection network exactly one of the three four-quadrant switches $\mathrm{S_{\bar{a}y\bar{a}}}$, $\mathrm{S_{\bar{b}y\bar{b}}}$, $\mathrm{S_{\bar{c}y\bar{c}}}$ is turned on during each grid voltage sector. Furthermore, the injection current i_{y} flows through one active switch and one diode of the turned-on four-quadrant switch. Which one of the two active switches and diodes is conducting depends on the sign of i_{y}. The same rms and average current stresses result for all four semiconductors of each four-quadrant switch due to phase symmetry. Considering only $i_{\mathrm{y}} > 0$ and the gird voltage sectors where $\mathrm{S_{\bar{a}y\bar{a}}}$ is on ($\pi/3 < \omega t < 2\pi/3$ and $4\pi/3 < \omega t < 5\pi/3$) the current in $\mathrm{S_{\bar{a}y\bar{a}}}$ can be expressed as

$$i_{\mathrm{S\bar{a}y\bar{a}}} = \begin{cases} I_{\mathrm{DC}} & \text{if } d_{\mathrm{n}} > d_{\mathrm{p}} \\ 0 & \text{otherwise}\,. \end{cases} \tag{19}$$

The rms and average current stresses can then be found by integration

$$I_{\mathrm{S\bar{k}y\bar{k},rms}} = I_{\mathrm{DC}} \sqrt{\frac{M_{\mathrm{d}}}{\pi} \left[\frac{1}{\cos(\phi)} - \frac{\sqrt{3}}{2} \right]} \; \forall \, \bar{k} \in \{\bar{a}, \bar{b}, \bar{c}\} \, , \tag{20}$$

$$I_{\mathrm{S\bar{k}y\bar{k},avg}} = I_{\mathrm{DC}} \frac{M_{\mathrm{d}}}{\pi} \left[\frac{1}{\cos(\phi)} - \frac{\sqrt{3}}{2} \right] \quad \forall \, \bar{k} \in \{\bar{a}, \bar{b}, \bar{c}\} \, . \tag{21}$$

If no reactive power is generated ($\phi = 0°$), the average current stress of the injection network switches $\mathrm{S}_{\bar{k}y\bar{k}}$ is $\approx 15\,\%$ of the average current stress of the rectifier diodes $\mathrm{D}_{\bar{k}x}$ and $\mathrm{D}_{z\bar{k}}$. The same value results for the ratio of squared rms currents. This implies that the conduction losses in the injection network switches $\mathrm{S}_{\bar{k}y\bar{k}}$ will typically be considerably lower than conduction losses in the rectifier diodes $\mathrm{D}_{\bar{k}x}$, $\mathrm{D}_{z\bar{k}}$ and corresponding parallel switches $\mathrm{S}_{x\bar{k}}$ and $\mathrm{S}_{\bar{k}z}$.

Note that the rms and average current in the current injection network increase with the absolute value of the phase shift angle ϕ. The maximum rms current, occurring for $\phi = \pm 30°$, is $\approx 47\,\%$ higher compared to $\phi = 0°$ while the average current current is $\approx 115\,\%$ higher. Therefore, the conduction losses in the injection network at $\phi = \pm 30°$ are ≈ 2.15 times the losses if no reactive power ($\phi = 0°$) is generated.

3) Passive Components: As shown above, the generation of the reactive power on the AC side does not influence the active power transferred to the DC side directly. Therefore, the current and voltage stresses of the buck converter inductors (L_{p}, L_{n}) and the output capacitor (C_{pn}) are almost independent of the reactive power generated on the AC side. Note that the AC side input currents i_{a}, i_{b}, i_{c} depend only on the modulation index M but not on the actual phase shift angle ϕ, as can be seen from **Fig. 4**:

$$I_{\mathrm{a,b,c}} = I_{\mathrm{DC}} \frac{M}{\sqrt{2}} \leq I_{\mathrm{DC}} \frac{1}{\sqrt{2}} \, . \tag{22}$$

Finally the rms current stress of the AC side input filter capacitors can be calculated from the equations derived above. During each gird voltage sector either one of the rectifier diodes $\mathrm{D}_{\bar{k}x}$, $\mathrm{D}_{z\bar{k}}$ or the injection switch $\mathrm{S}_{\bar{k}y\bar{k}}$ is conducting. Therefore the corresponding rms currents can be combined using Pythagorean addition (cf. **Fig. 10**, $k = a$, $\bar{k} = \bar{a}$)

$$I_{\mathrm{C\bar{k},rms}} = \sqrt{\underbrace{I^2_{\mathrm{D\bar{k}x,rms}} + I^2_{\mathrm{Dz\bar{k},rms}} + 2\, I^2_{\mathrm{S\bar{k}y\bar{k},rms}}}_{I^2_{\mathrm{\bar{k},rms}}} - I^2_{\mathrm{k}}} \tag{23}$$

$$= I_{\mathrm{DC}} \sqrt{\frac{2}{\pi} M - \frac{1}{2} M^2} \, . \tag{24}$$

It can be seen that the filter capacitor's rms current stress depends on the modulation index $M \in [0;1]$ but not on the phase shift angle ϕ. The highest rms current stress, which is typically required for the dimensioning of a rectifier system, can be calculated as

$$I_{\mathrm{C\bar{k},rms}}\,(M) \leq I_{\mathrm{DC}} \frac{\sqrt{2}}{\pi} \approx 0.45\, I_{\mathrm{DC}} \, . \tag{25}$$

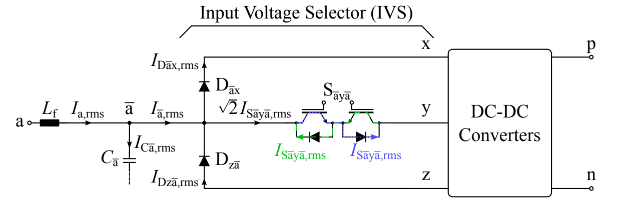

Fig. 10. Simplified schematic of the IVS, showing the rms currents used to calculate the filter capacitor current's rms value $I_{\mathrm{C\bar{a},rms}}$. Phases b and c are omitted for clarity.

4) Numerical Results: In **Table II** numerical simulation results for the rms and average current stresses are compared to the corresponding values calculated using the analytical equations derived above. Two operating points, one with purely active power ($\phi = 0°$) and one with maximum reactive power ($\phi = 30°$) are shown. In both cases the deviation between value calculated with the analytical formula and the simulation result is less than 3.4 %. Accordingly, the analytical expressions can directly be used for dimensioning the system.

TABLE II
COMPARISON OF CALCULATED AND SIMULATED CURRENT STRESSES

	Calculation	Simulation	Deviation
ϕ	0°		
I_{DC}	18.75 A		
M	83.3 %		
$I_{\mathrm{Sx\bar{p},rms}}$	15.6 A	15.6 A	−0.2 %
$I_{\mathrm{Sx\bar{p},avg}}$	12.9 A	12.9 A	−0.1 %
$I_{\mathrm{Dy\bar{p},rms}}$	10.5 A	10.4 A	0.3 %
$I_{\mathrm{Dy\bar{p},avg}}$	5.83 A	5.81 A	0.3 %
$I_{\mathrm{D\bar{k}x,rms}}$	8.98 A	9.01 A	−0.3 %
$I_{\mathrm{D\bar{k}x,avg}}$	4.31 A	4.32 A	−0.3 %
$I_{\mathrm{S\bar{k}y\bar{k},rms}}$	3.53 A	3.53 A	0.3 %
$I_{\mathrm{S\bar{k}y\bar{k},avg}}$	0.67 A	0.69 A	−3.4 %
$I_{\mathrm{C\bar{k},rms}}$	8.03 A	8.20 A	−2.3 %
ϕ	30°		
I_{DC}	18.75 A		
M	96.2 %		
$I_{\mathrm{Sx\bar{p},rms}}$	15.6 A	15.6 A	−0.1 %
$I_{\mathrm{Sx\bar{p},avg}}$	12.9 A	12.9 A	0.0 %
$I_{\mathrm{Dy\bar{p},rms}}$	10.5 A	10.4 A	0.3 %
$I_{\mathrm{Dy\bar{p},avg}}$	5.83 A	5.81 A	0.4 %
$I_{\mathrm{D\bar{k}x,rms}}$	8.98 A	8.99 A	−0.1 %
$I_{\mathrm{D\bar{k}x,avg}}$	4.31 A	4.31 A	0 %
$I_{\mathrm{S\bar{k}y\bar{k},rms}}$	5.19 A	5.17 A	0.3 %
$I_{\mathrm{S\bar{k}y\bar{k},avg}}$	1.44 A	1.43 A	0.4 %
$I_{\mathrm{C\bar{k},rms}}$	7.26 A	7.44 A	−2.4 %

III. OPERATION WITH UNSYMMETRIC MAINS VOLTAGES

So far, the AC grid voltages were assumed to be purely sinusoidal, of equal amplitude and shifted by 120°. However, real AC distribution girds typically exhibit several percent of low frequency harmonics and an asymmetry of the phase voltages. In this section control strategies for constant output power and resistive mains behavior are analyzed.

A. Constant Power Transfer

It can be seen from the schematic shown in **Fig. 6** that the power transferred to the rectifier's DC output is given by

$$p_{\mathrm{DC}}(t) = u_{\mathrm{pn}}(t)\, i_{\mathrm{DC}}(t) \, . \tag{26}$$

If the output voltage controller $R(s)$ and the current controller $G(s)$ have settled, p_{DC} will be constant for stationary

operation and constant load. Furthermore, the power delivered to the DC bus is almost independent of the AC grid voltages in this case. Hence, this control scheme allows an operation of the converter with the minimal DC output filter capacitance C_{pn}.
The power drawn from the AC grid by the SWISS Rectifier is given by equation (27). If losses in the converter are neglected, the power drawn from the AC gird has to be equal to the power delivered to the DC output, as the Input Voltage Selector and the DC-DC converters contain only switching frequency energy storage elements.

$$p_{\text{AC}}(t) = u_{\text{a}}(t)\, i_{\text{a}}(t) + u_{\text{b}}(t)\, i_{\text{b}}(t) + u_{\text{c}}(t)\, i_{\text{c}}(t) \tag{27}$$
$$p_{\text{AC}}(t) = p_{\text{DC}}(t) = p(t) \tag{28}$$

If the AC grid voltages $u_{\text{a,b,c}}$ are asymmetrical, e.g. if the amplitudes of the individual phase voltages are not equal, constant AC side power $p_{\text{AC}} = p_{\text{DC}}$ can only be achieved with non-sinusoidal grid currents $i_{\text{a,b,c}}$.

B. Constant Input Resistance

In certain applications the rectifier system might be required to behave like a symmetrical resistive load even with unsymmetrical grid voltages. In this case the AC side input currents $i_{\text{a,b,c}}$ are given by equation (29). R_{in} is the resistance of one phase of a fundamental frequency rectifier equivalent circuit for star connection. Note that, since the converter has no connection to the AC grid's neutral N, no zero sequence current $i_0 = (i_{\text{a}} + i_{\text{b}} + i_{\text{c}})/3$ can be created by the rectifier. Therefore only the positive and negative sequence components $u'_{\text{a,b,c}}$ of the grid voltages u_1 contribute to the power flow and hence equation (30) results.

$$i_{\text{k}}(t) = \frac{u_{\text{k}}(t)}{R_{\text{in}}} \quad \forall\, k \in \{a, b, c\} \tag{29}$$
$$p_{\text{AC}}(t) = \frac{1}{R_{\text{in}}}\left[u_{\text{a}}'^{2}(t) + u_{\text{b}}'^{2}(t) + u_{\text{c}}'^{2}(t)\right] \tag{30}$$

Due do the balance of power on the AC and DC side of the converter and equation (26), the DC side output current $i_{\text{DC}}(t)$ has to be proportional to $p_{\text{AC}}(t)$. This can be achieved with the control structure shown in **Fig. 11**. The output signal I^*_{DC} of the DC voltage controller $R(s)$ is multiplied with a shaping signal m in order to derive the DC link current reference for the current controller. No changes are required to the current control loop shown in **Fig. 6**. The signal m is calculated by subtracting the zero sequence system of the measured input voltages $u_{\text{a,b,c}}$ and summing their squares. A scaling factor of $2/3\,\hat{U}^2_{1,\text{pos}}$ is used, where $\hat{U}_{1,\text{pos}}$ is the amplitude of the first harmonic positive sequence system. This ensures $m = 1$ for symmetrical phase voltages with nominal amplitude $\hat{U}_1 = \hat{U}_{1,\text{pos}}$.

In **Fig. 12** simulation results are shown for the SWISS Rectifier specified in **Table I**, operated at a AC grid where the voltage amplitude of phase a is 23 V higher than on phases b and c. Until $t = 30\,\text{ms}$ the converter operates with the control structure shown in **Fig. 6** (i.e. $m = 1$), causing low frequency distortions of the input currents due to the constant instantaneous power flow requirement. At $t = 30\,\text{ms}$ the control system is changed to the structure shown in **Fig. 11**. Therefore, the AC side input currents are now sinusoidal and i_{a} has a higher amplitude than i_{b} and i_{c} as expected from (29). Furthermore the DC current reference signal i^*_{DC} is no longer constant due to the instantaneous power flow pulsating with twice the mains frequency.

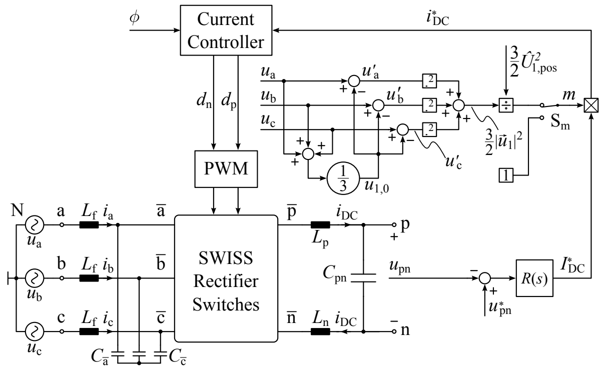

Fig. 11. Modified control structure allowing ohmic mains behavior for asymmetrical mains voltages $u_{\text{a,b,c}}$. The output I^*_{DC} of the DC voltage controller $R(s)$ is rescaled with a signal m which is proportional to the square of the instantaneous amplitude of the input voltage space vector $|\vec{u_1}|^2$. The same inner loop current controller as in **Fig. 6** is used.

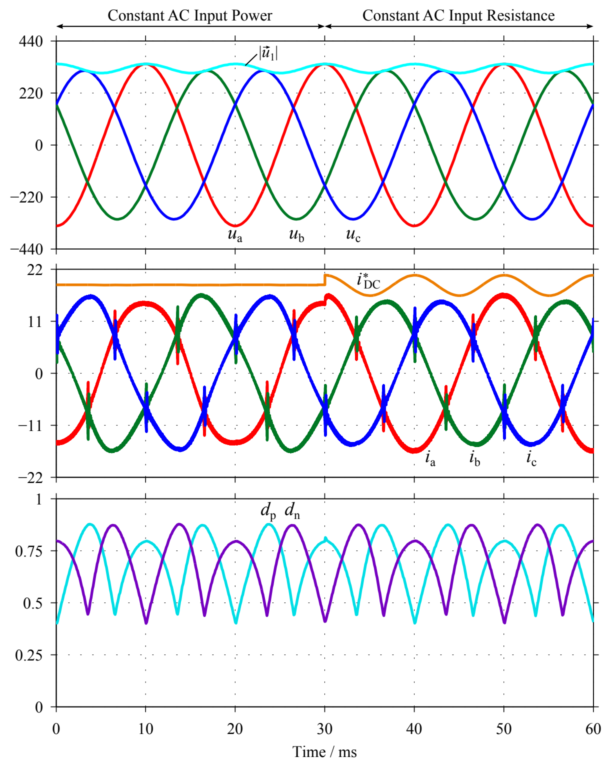

Fig. 12. Simulated mains phase voltages $u_{\text{a,b,c}}$, input phase currents $i_{\text{a,b,c}}$, DC inductor current reference i^*_{DC} and DC-DC converter duty cycles d_{p} and d_{n} for an AC grid containing 19 V first harmonic negative sequence voltage. The rectifier transfers nominal power (7.5 kW) from the AC to the DC side. Until $t = 30\,\text{ms}$ the converter is operated with constant instantaneous AC side input power, afterwards with constant AC side input resistance.

IV. Implementation Results

A SWISS Rectifier prototype has been built according to the specifications given in **Table I**, a picture of the prototype hardware is shown in **Fig. 14**. The values of all major components match those used for creating the simulation results shown in the previous sections. Measurements taken on this prototype are presented in the following.

A. Phase Shifted AC Currents

Figure 15 shows measurement results for AC-to-DC power transfer at 7.3 kW DC output power. Note that the

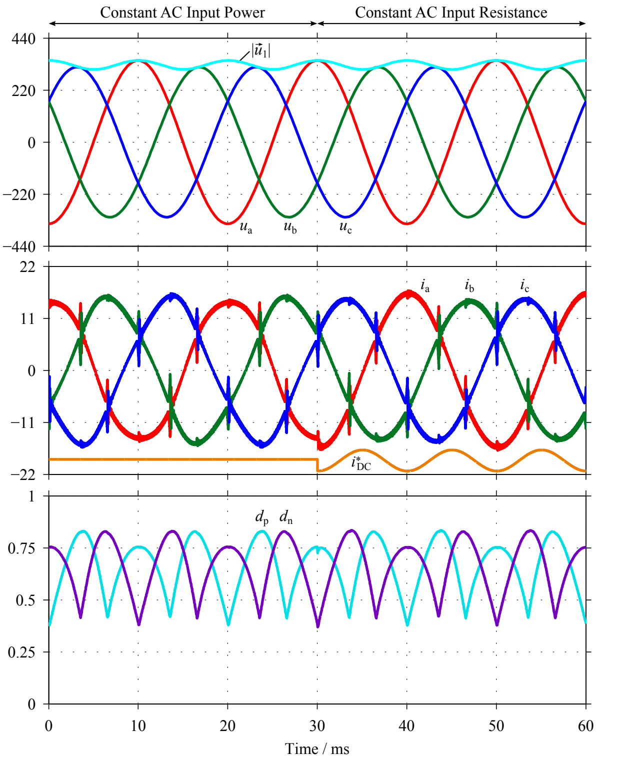

Fig. 13. Simulated mains phase voltages $u_{\mathrm{a,b,c}}$, input phase currents $i_{\mathrm{a,b,c}}$, DC inductor current reference i^{*}_{DC} and DC-DC converter duty cycles d_{p} and d_{n} for an AC mains containing 19 V first harmonic negative sequence voltage. The rectifier transfers nominal power (7.5 kW) from the DC to the AC side. Until $t = 30\,\mathrm{ms}$ the converter is operated with constant instantaneous AC side input power, afterwards with constant AC side input resistance.

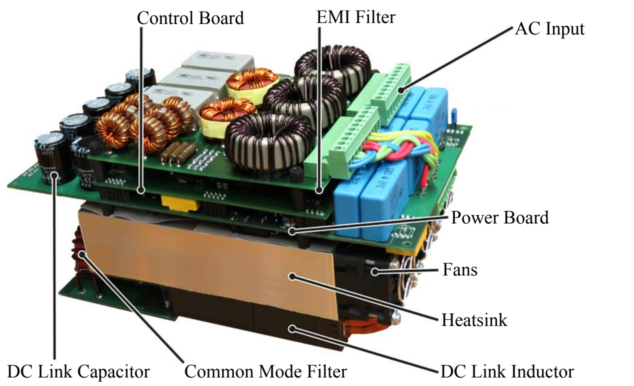

Fig. 14. Picture of the implemented 7.5 kW bidirectional SWISS Rectifier prototype hardware.

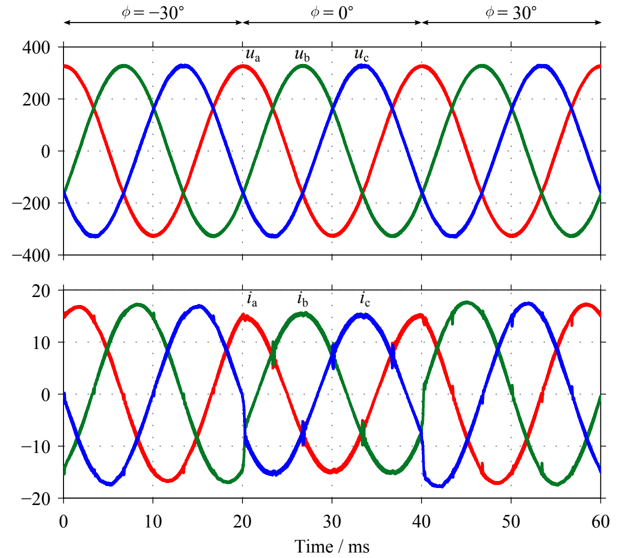

Fig. 15. Meaurement results for AC-to-DC power transfer, showing grid voltages $u_{\mathrm{a,b,c}}$ and input currents $i_{\mathrm{a,b,c}}$ for $\phi = -30°$ (inductive), $\phi = 0°$ (ohmic) and $\phi = 30°$ (capacitive) AC side currents. Note that phase quantities a and b were measured directly, phase c was recreated numerically as $u_{\mathrm{c}} = -u_{\mathrm{a}} - u_{\mathrm{b}}$ and $i_{\mathrm{c}} = -i_{\mathrm{a}} - i_{\mathrm{b}}$.

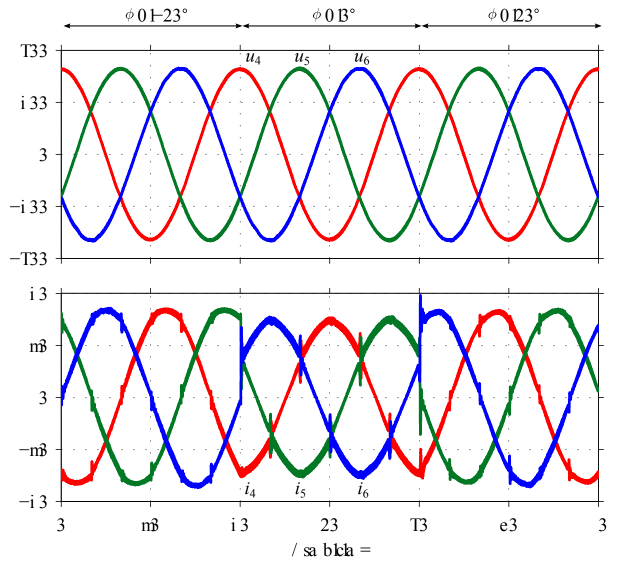

Fig. 16. Meaurement results for DC-to-AC power transfer, showing grid voltages $u_{\mathrm{a,b,c}}$ and input currents $i_{\mathrm{a,b,c}}$ for $\phi = -30°$ (inductive), $\phi = 0°$ (ohmic) and $\phi = 30°$ (capacitive) AC side currents. Note that phase quantities a and b were measured directly, phase c was recreated numerically as $u_{\mathrm{c}} = -u_{\mathrm{a}} - u_{\mathrm{b}}$ and $i_{\mathrm{c}} = -i_{\mathrm{a}} - i_{\mathrm{b}}$.

voltage and current of phases a and b where measured directly while the quantities for phase c were recreated assuming $u_{\mathrm{a}} + u_{\mathrm{b}} + u_{\mathrm{c}} = 0$ and $i_{\mathrm{a}} + i_{\mathrm{b}} + i_{\mathrm{c}} = 0$. During the first gird voltage period ($0 < t < 20\,\mathrm{ms}$) the converter is operated with a phase shift of $\phi = -30°$ resulting in inductive behavior. At $t = 20\,\mathrm{ms}$ the phase shift angle ϕ is set to zero resulting in almost purely active power drawn from the AC grid. The remaining capacitive reactive power is caused by the input filter. Finally ϕ is set to 30° at $t = 40\,\mathrm{ms}$ resulting in capacitive behavior in the third grid voltage period shown.

The same sequence of input current phase angle steps as described above has been applied for DC-to-AC power transfer (7.5 kW) in the measurement shown in **Fig. 16**. For both, AC-to-DC and DC-to-AC power transfer, sinusoidal AC side currents result for all tested values of ϕ.

B. Operation Under Unsymmetrical Mains Voltages

In order to test the operation of the SWISS Rectifier under unsymmetrical AC grid voltages the control structure proposed in **Section III** is implemented. A three-phase grid containing a first harmonic negative sequence voltage component with an amplitude of 19 V is used for the measurements. Note that no DC output voltage controller was used, the DC voltage u_{pn} was defined by a constant voltage source (or sink) instead.

Measurement results for AC-to-DC power transfer are shown in **Fig. 17**. During the first 30 ms the converter is operated with constant AC side input power resulting in non-sinusoidal grid currents $i_{\mathrm{a,b,c}}$. At $t = 30\,\mathrm{ms}$ the control

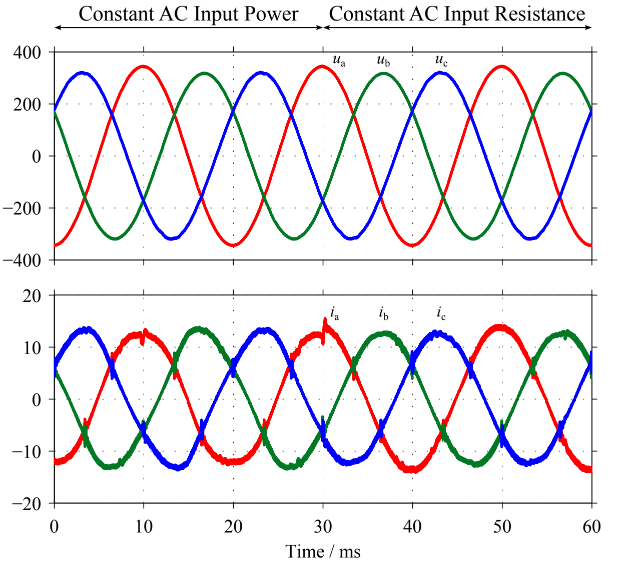

Fig. 17. Meaurement results for AC-to-DC power transfer, showing unsymmetrical grid voltages $u_{\mathrm{a,b,c}}$ and input currents $i_{\mathrm{a,b,c}}$ for constant instantaneous AC power and ohmic mains behavior. Note that phase quantities a and b were measured directly, phase c was recreated numerically as $u_{\mathrm{c}} = -u_{\mathrm{a}} - u_{\mathrm{b}}$ and $i_{\mathrm{c}} = -i_{\mathrm{a}} - i_{\mathrm{b}}$.

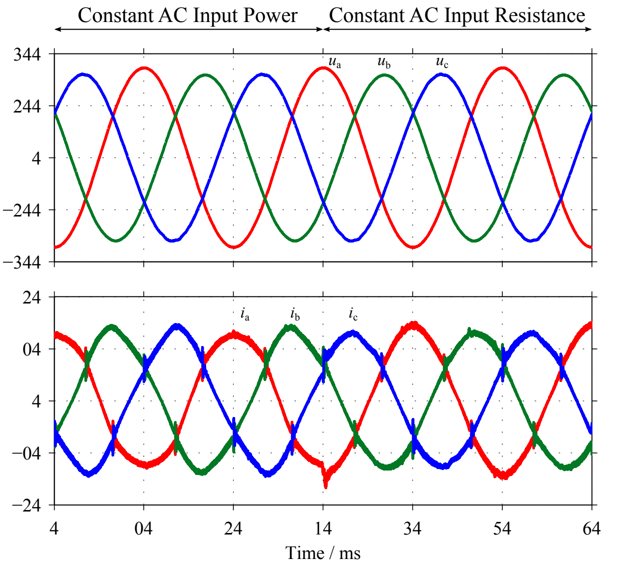

Fig. 18. Meaurement results for DC-to-AC power transfer, showing grid voltages $u_{\mathrm{a,b,c}}$ and input currents $i_{\mathrm{a,b,c}}$ for constant instantaneous AC power and ohmic mains behavior. Note that phase quantities a and b were measured directly, phase c was recreated numerically as $u_{\mathrm{c}} = -u_{\mathrm{a}} - u_{\mathrm{b}}$ and $i_{\mathrm{c}} = -i_{\mathrm{a}} - i_{\mathrm{b}}$.

structure is changed to ohmic mains behavior, resulting in sinusoidal grid currents. Furthermore the amplitude of i_{a} increases in order to achieve equal input resistance at all three phases.

The same measurement, with DC-to-AC power transfer, is shown **Fig. 18**. Again the SWISS Rectifier operates with constant AC power during $0 < t < 30\,\mathrm{ms}$ and with constant AC resistance during $30\,\mathrm{ms} < t < 60\,\mathrm{ms}$.

V. Conclusion

In this paper a control structure for uni- and bidirectional SWISS Rectifiers is proposed, which allows the AC side input currents to be shifted up to $\pm 30°$ with respect to the mains' phase voltages. This allows the generation of reactive power on the AC side, which e.g. could be used to compensate the reactive power demand of the input filter or for compliance with grid codes demanding reactive power generation under certain conditions. However, the generation of reactive power reduces the output voltage range of the rectifier system.

Furthermore, analytical equations for the resulting rms and average current stresses of the converter's switches and passive components are derived for reactive power generation. The resulting formulas show that the rms current stress in the injection network's four quadrant switches increases from $0.21\,I_{\mathrm{DC}}$ if no reactive power is generated to $0.30\,I_{\mathrm{DC}}$ at $\phi = 30°$. The corresponding average current stress increases from $0.04\,I_{\mathrm{DC}}$ to $0.09\,I_{\mathrm{DC}}$. The conduction and switching losses of all other semiconductors, including the IVS' full wave diode bridge, are not affected by the generation of reactive power.

Additionally, the operation of a SWISS Rectifier with unsymmetrical mains voltages has been analyzed. A proposed extension to the control structure allows the SWISS Rectifier to achieve ohmic mains behavior or constant power transfer even if the AC input voltages are unbalanced.

Simulations and measurements taken on a 7.5 kW laboratory prototype SWISS Rectifier demonstrate the feasibility of the proposed concepts.

Acknowledgment

The authors would like to thank ABB Switzerland Ltd. for the funding and for their support regarding many aspects of this research project.

References

[1] D. Aggeler, F. Canales, H. Zelaya-De La Parra, A. Coccia, N. Butcher and O. Apeldoorn, "Ultra-Fast DC-Charge Infrastructures for EV-Mobility and Future Smart Grids," in *Proc. of IEEE Innovative Smart Grid Technologies Conference Europe (ISGT)*, Oct 2010, pp. 1–8.

[2] H. Kakigano, Y. Miura and T. Ise, "Low-Voltage Bipolar-Type DC Microgrid for Super High Quality Distribution," *IEEE Transactions on Power Electronics*, vol. 25, no. 12, pp. 3066–3075, Dec 2010.

[3] A. Pratt, P. Kumar and T. V. Aldridge, "Evaluation of 400V DC Distribution in Telco and Data Centers to Improve Energy Efficiency," in *Proc. of IEEE Telecommunications Energy Conference (INTELEC)*, Sept 2007, pp. 32–39.

[4] G. AlLee and W. Tschudi, "Edison Redux: 380 Vdc Brings Reliability and Efficiency to Sustainable Data Centers," *IEEE Power and Energy Magazine*, vol. 10, no. 6, pp. 50–59, Nov 2012.

[5] J. W. Kolar and T. Friedli, "The Essence of Three-Phase PFC Rectifier Systems - Part I," *IEEE Transactions on Power Electronics*, vol. 28, no. 1, pp. 176–198, Jan 2013.

[6] T. B. Soeiro, T. Friedli and J. W. Kolar, "Swiss Rectifier - A Novel Three-Phase Buck-Type PFC Topology for Electric Vehicle Battery Charging," in *Proc. of IEEE Applied Power Electronics Conference and Exposition (APEC)*, Feb 2012, pp. 2617–2624.

[7] M. F. Vancu, T. B. Soeiro, J. Mühlethaler, J. W. Kolar and D. Aggeler, "Comparative Evaluation of Bidirectional Buck-Type PFC Converter Systems for Interfacing Residential DC Distribution Systems to the Smart Grid," in *Proc. of IEEE Industrial Electronics Society Conference (IECON)*, Oct 2012, pp. 5153–5160.

[8] L. Malesani and P. Tenti, "Three-Phase AC/DC PWM Converter with Sinusoidal AC Currents and Minimum Filter Requirements," *IEEE Transactions on Industry Applications*, vol. IA-23, no. 1, pp. 71–77, Jan 1987.

[9] S. Hiti, V. Vlatkovic, D. Borojevic, and F. C. Lee, "A New Control Algorithm for Three-Phase PWM Buck Rectifier with Input Displacement Factor Compensation," *IEEE Transactions on Power Electronics*, vol. 9, no. 2, pp. 173–180, Mar 1994.